



Bubble dynamics in various commercial sparkling bottled waters



G erard Liger-Belair^{a,*}, Florine Sternenberg^b, St ephane Brunner^b, Bertrand Robillard^c, Clara Cilindre^a

^a *Equipe Effervescence, Champagne et Applications (GSMA), UMR CNRS 7331, Universit e de Reims Champagne-Ardenne, BP 1039, 51687 Reims Cedex 2, France*

^b *Danone Research, Centre de Recherche Daniel Carasso, RD 128, 91767 Palaiseau, France*

^c *Institut C enologique de Champagne (IOC), ZI de Mardeuil, Route de Cumi eres, BP 25, 51201 Epernay Cedex, France*

ARTICLE INFO

Article history:

Received 3 February 2015

Received in revised form 31 March 2015

Accepted 19 April 2015

Available online 24 April 2015

Keywords:

CO₂

Sparkling waters

Bubble dynamics

Molecular diffusion

ABSTRACT

Observations were made relevant to common situations involving the service of various sparkling waters. Bubble dynamics and progressive losses of dissolved CO₂ were closely examined in three various batches of carbonated waters holding different levels of CO₂. During the turbulences of the pouring process, a cloud of bubbles appears in the water bulk. Under the action of buoyancy, bubbles progressively reach the free surface, and the cloud of bubbles finally vanishes. Bubbles also nucleate on the glass wall, where they grow by diffusion until buoyancy forces them to detach and rise to the free surface to release their CO₂. The three batches of sparkling waters were clearly differentiated with regard to their bubbles dynamics and losses of dissolved CO₂. Our observations were systematically rationalized and discussed on the basis of mass transfer considerations including molecular diffusion, basic concepts of gas solution thermodynamic equilibrium, and bubble dynamics.

  2015 Elsevier Ltd. All rights reserved.

1. Introduction

In the past 15 years, the global bottled water market has seen a remarkable growth (Euzen, 2006; Storey, 2010; Rani et al., 2012), thus raising in turn legitimate environmental concerns regarding the waste management sector (Gleick, 2010). The Forbes magazine even declared that bottled water is expected to become the largest segment of the U.S. liquid refreshment beverage market by the end of this decade (Forbes, 2014). In 2011, the global bottled water market has reached 233 billion liters sold all over the world (Rodwan, 2012).

Among the global bottled water, the sparkling water segment represents nowadays about 10% of the whole bottled water industry. Nevertheless, this percentage may vary a lot from country to country. In the UK, it is close to the global average, whereas in Germany, which is the biggest bottled water market in the world for premium waters, around 80% of the market is actually sparkling waters (Euzen, 2006). Sparkling waters are often seen as a substitute for sweet beverages, and this is particularly true for flavored sparkling waters (Rani et al., 2012). Suffice to say that the bottled sparkling water is a booming, but very competitive market, involving numerous companies throughout the world, with Europe being the largest producer (75%), followed by the USA (20%) (Bruce, 2013).

Classification and labeling of bottled carbonated waters must be in conformity with EU regulations (E. Directive 2009/54/EC and 2003/40/EC). Commercial bottled carbonated natural mineral waters fall into three categories: (1) "naturally carbonated natural mineral water", when the water content of carbon dioxide coming from the spring, and in the bottle are the same as at source; (2) "natural mineral water fortified with gas from the spring" if the content of carbon dioxide comes from the same resource, but its content in the bottle is greater than the one established at source; and (3) "carbonated natural mineral water" if carbon dioxide from an origin other than the groundwater resource is added. Actually, a method using gas chromatography-isotope ratio mass spectrometry has been proposed to determine the carbon isotope ratio ¹³C/¹²C of CO₂ (Calderone et al., 2007). This method was successfully applied to differentiate whether or not gaseous CO₂ in the headspace of a bottled carbonated water originates from the source spring or is of industrial origin.

The capacity of CO₂ to get dissolved in water is ruled by the well-known Henry's law, which states that the equilibrium concentration *c* of dissolved CO₂ is proportional to the partial pressure of gas phase CO₂ denoted *P*:

$$c = k_H P \quad (1)$$

with *k_H* being the strongly temperature-dependent Henry's law constant of gaseous CO₂ in water (i.e., its solubility) (Carroll and Mather, 1992; Diamond and Akinfief, 2003). Under identical conditions of temperature, water can therefore hold different levels of

* Corresponding author.

E-mail address: gerard.liger-belair@univ-reims.fr (G. Liger-Belair).

Nomenclature

c_L	concentration of dissolved CO ₂ in the liquid phase, in g L ⁻¹	k_H	Henry's law constant of dissolved CO ₂ in water (i.e., its solubility), in g L ⁻¹ bar ⁻¹
c_0	concentration of dissolved CO ₂ in Henry's equilibrium with gas phase CO ₂ in the bubble, in g L ⁻¹	m	cumulative mass of CO ₂ escaping the liquid phase, in g
c_i	initial concentration of dissolved CO ₂ in the liquid phase, in g L ⁻¹	M	molar mass of CO ₂ , =44 g mol ⁻¹
d	bubble diameter, in m	n	mole number of gaseous CO ₂ in the bubble, in mol
D	diffusion coefficient of dissolved CO ₂ in the liquid phase, in m ² s ⁻¹	P	pressure, in Pa
F_T	total volume flux of gaseous CO ₂ escaping the liquid phase, in cm ³ s ⁻¹	r	bubble radius, in m
g	gravity acceleration, in m s ⁻²	R	ideal gas constant, =8.31 J K ⁻¹ mol ⁻¹
h	level of liquid in the glass, in m	t	time, in s
J	molar flux of gaseous CO ₂ which crosses the bubble interface, in mol ⁻¹ m ⁻² s ⁻¹	T	temperature, in K
k	growth rate of bubbles growing through molecular diffusion in the liquid phase supersaturated with dissolved CO ₂ , in m s ⁻¹	U	ascending bubble velocity, in m s ⁻¹
		v	bubble volume, in m ³
		V	volume of liquid poured into the glass or plastic goblet, in L
		λ	thickness of the diffusion boundary layer around the bubble, in m
		η	dynamic viscosity of water, in Pa s
		ρ	density of water, in kg m ⁻³

dissolved CO₂, depending on the pressure of gas phase CO₂ found in the headspace below the cap or screw cap.

In carbonated beverages, the concentration of dissolved CO₂ is indeed a parameter of paramount importance since it is responsible for the very much sought-after fizzy sensation, and bubble formation (the so-called *effervescence*). In sparkling waters, and carbonated beverages in general, homogeneous bubble nucleation (*ex nihilo*) is thermodynamically forbidden (Wilt, 1986; Lubetkin, 2003). In order to nucleate, bubbles need preexisting gas cavities immersed in the liquid phase, with radii of curvature larger than a critical size. In carbonated beverages typically holding several grams per liter of dissolved CO₂, the critical radius needed to initiate bubble nucleation (under standard conditions for pressure and temperature) is of order of 0.1–0.2 μm (Liger-Belair, 2014). This non-classical heterogeneous bubble nucleation process is referred to as type IV nucleation, following the classification by Jones et al. (1999). The presence of dissolved CO₂ therefore directly impacts consumers of sparkling waters, by impacting several emblematic sensory properties such as (i) the visually appealing frequency of bubble formation (Liger-Belair et al., 2006), (ii) the growth rate of bubbles ascending in the glass (Liger-Belair, 2012), and (iii) the very characteristic tingling sensation in mouth. Carbonation, or the perception of dissolved CO₂, indeed involves a truly very complex multimodal stimulus (Lawless and Heymann, 2010). During carbonated beverage tasting, dissolved CO₂ acts on both trigeminal receptors (Dessirier et al., 2000; Kleeman et al., 2009; Meusel et al., 2010), and gustatory receptors, via the conversion of dissolved CO₂ to carbonic acid (Chandrashekar et al., 2009; Dunkel and Hofmann, 2010), in addition to the tactile stimulation of mechanoreceptors in the oral cavity (through bursting bubbles). More recently, Wise et al. (2013) showed that the carbonation bite was rated equally strong with or without bubbles under normal or higher atmospheric pressure, respectively. However, a consumer preference for carbonated water containing smaller bubbles has been previously reported in a thorough study on the nucleation and growth of CO₂ bubbles following depressurisation of a saturated carbon dioxide/water solution (Barker et al., 2002). Moreover, it was also clearly reported that high levels of inhaled gaseous CO₂ become irritant in the nasal cavity (Cain and Murphy, 1980; Cometto-Muniz et al., 1987).

For all the aforementioned reasons, monitoring accurately the losses of dissolved CO₂ in a glass poured with sparkling water is

of interest for carbonated waters elaborators. In the past 15 years, the physics and chemistry behind effervescence has indeed been widely investigated in champagne and sparkling wines (for a recent and global overview, see Liger-Belair (2012) and references therein). Nevertheless, and to the best of our knowledge, the bubbling process itself and the release of gaseous CO₂ remained poorly explored in sparkling waters, under standard tasting conditions.

The present article reports experimental observations relevant to common situations involving the service of commercial carbonated natural mineral bottled waters. Bubble dynamics and progressive losses of dissolved CO₂ were closely examined in three various batches of naturally carbonated waters holding different levels of CO₂. Our observations were conducted in real consuming conditions, i.e., in a glass and in a plastic goblet. During the pouring process, a cloud of bubbles nucleate and grow in the water bulk. Under the action of buoyancy, bubbles rise toward the free surface, and the cloud of bubbles progressively vanishes. Bubbles also nucleate on the glass wall, where they grow by diffusion until buoyancy forces them to detach and rise toward the free surface. We explored the above questions with dedicated experiments used to quantify the bubble dynamics, and the kinetics of gaseous CO₂ discharging from the liquid phase (in real consuming conditions) as described in Section 2. In Section 3.1., the lifetime of the quickly vanishing cloud of bubbles following the pouring step is examined. In Section 3.2., the progressive losses of dissolved CO₂ escaping from the liquid phase (once it is poured in a plastic goblet) are measured and discussed. Finally, in Section 3.3., kinetics of bubbles growing stuck on the plastic goblet are closely examined. Our observations are rationalized and discussed on the basis of mass transfer considerations including molecular diffusion, basic concepts of gas solution thermodynamics, and ascending bubble dynamics.

2. Materials and methods

2.1. The three batches of carbonated waters

Three batches of various commercial carbonated natural mineral bottled waters from Poland, and provided by Danone Research, were investigated. They are described and referenced as follows:

Table 1

Physicochemical pertinent properties of the three carbonated waters investigated in this study, namely, dissolved CO₂, and non-CO₂ gases (O₂ and N₂) initially held in the closed PET bottled waters, as well as their dynamic viscosity.

Water sample	[CO ₂] c _i (g L ⁻¹)	Non-CO ₂ gases (O ₂ /N ₂) (mg L ⁻¹)	Viscosity η (×10 ⁻³ Pa s)
LCW	3.25 ± 0.08	17	0.98 ± 0.01
MCW	4.53 ± 0.15	8.5	0.99 ± 0.01
HCW	6.87 ± 0.28	9.5	0.99 ± 0.01

1. A low carbonated water (labeled LCW);
2. A medium carbonated water (labeled MCW); and
3. A highly carbonated water (labeled HCW).

MCW and HCW are conditioned in 1.5 l polyethylene terephthalate (PET) bottles, whereas LCW is conditioned in 0.7 l PET bottles. Concentrations of dissolved CO₂ found in water samples were determined by using carbonic anhydrase (labeled C2522 Carbonic Anhydrase Isozyme II from bovine erythrocytes, and provided from Sigma–Aldrich – US) (Caputi et al., 1970). This method is thoroughly detailed in a previous paper (Liger-Belair et al., 2009). Non-CO₂ gases (O₂ and N₂) were also approached through measurements based on the multiple volume expansion method (MVE) deduced from a typical CarboQC beverage carbonation meter (Anton Paar). Moreover, for each water sample, the dynamic viscosity (denoted η) was measured, at 20 °C, with an Ubbelohde capillary viscometer, and with water samples first degassed under vacuum. Table 1 compiles the pertinent data discussed in this study. Actually, because the level of dissolved gases is the main cause behind bubble nucleation and growth in sparkling beverages (Liger-Belair, 2012), it is worth noting that the very low concentrations of other “non CO₂” dissolved gases (with regard to the relatively high concentrations of dissolved CO₂ in water samples) has absolutely no impact considering the dynamics of CO₂ bubbles in these sparkling waters (even with the LCW, which contains twice as much other non-CO₂ dissolved gases than the two others water samples).

2.2. The glasses used and their washing protocol

Experiences dealing with the cloud of bubbles following the pouring step were conducted with a series of four «classical flutes» (180 mL – Marianna, Lednické, Slovakia/sold by Arystal), with an open aperture diameter of 4.8 cm, and a wall thickness of 0.8 mm. This glass model was chosen since it is perfectly cylindrical (i.e., with low optical distortion), and since it was specifically used, during the past few years, for the study of effervescence and foam formation in various standard commercial hydroalcoholic beverages supersaturated with dissolved CO₂ (Liger-Belair, 2012). Nevertheless, as concerns the kinetics of gas discharging from the liquid phase, as well as the kinetics of bubble growth on the glass wall, it did not seem perfectly adapted (due to a lack of reproducibility). Regarding the kinetics of gas discharging as well as the study of bubble growth on the glass wall, we rather used a simple plastic goblet (200 mL in volume), which showed a much more satisfying reproducibility from one pouring to another (with an identical water sample). Before each series of experiments dealing with the cloud of bubbles following the pouring process, flutes were carefully rinsed using distilled water and then compressed air-dried. Nevertheless, in case of the plastic goblets, goblets were used only once, and replaced before each new experimental data series.

2.3. Measuring the lifetime of quickly vanishing clouds of bubbles following pouring

Flutes were simply placed on a table, in front of a cold backlight. 180 ± 5 mL of water are poured into the flute standing vertically. Pouring series were conducted at room temperature (20 ± 1 °C). During the pouring step, which lasts approximately 5 s, water falls from the bottleneck, which stands about 1 cm above the upper part of the flute, as shown in the time-sequence displayed in Fig. 1. During the pouring process, a cloud of bubbles appears in the liquid phase, progressively rise toward the water surface under the action of buoyancy, and progressively vanishes as bubbles reach the free surface. Once the flute is filled with water, the lifetime of the cloud of bubbles is measured by use of a standard chronometer. The cloud of bubbles was clearly identified (by the naked eye) by use of the cold backlight placed behind the flute, which provides an excellent contrast between bubbles and water. To enable a statistical treatment, six successive pourings were done (from a single bottle), for each sparkling water sample, to finally produce one single “average” cloud of bubbles’ lifetime, characteristic of a given water sample (with standard deviations corresponding to the root-mean-square deviations of the values provided by the six successive data recordings).

2.4. Measuring the kinetics of dissolved CO₂ progressively discharging from water

100 ± 2 mL of sparkling water were poured into a goblet, previously level-marked with 100 mL of distilled water. Experiments were performed at room temperature (20 ± 1 °C). Immediately after pouring, the goblet was placed on the chamber base plate of a precision weighing balance (Sartorius – Extend Series ED) with a total capacity of 220 g and a standard deviation of ±0.001 g. The Sartorius balance was interfaced with a laptop PC recording data every 5 s from the start signal, activated just after the goblet was placed on the weighting chamber base plate. The total cumulative mass loss experienced by the goblet poured with water was recorded during the first 10 min following pouring. Actually, the mass loss of the goblet poured with water is the combination of both (i) water evaporation, and (ii) dissolved CO₂ progressively desorbing from the supersaturated liquid phase. The mass loss attributed to water evaporation only was simply accessible by recording the mass loss of a goblet poured with a sample of 100 mL of water first degassed under vacuum. Due to likely variations in hygrometric conditions from one day to another, standard evaporation was thus measured with a sample of water first degassed under vacuum, just before each series of total mass loss recordings was done. The cumulative mass loss vs. time attributed only to CO₂ molecules progressively desorbing from a sparkling water sample may therefore easily be accessible by subtracting the data series attributed to evaporation only from the total mass loss data series. Generally speaking, in the area of sparkling beverage, the parameter which characterizes a sample is its dissolved CO₂ concentration, denoted c_L, and usually expressed in g L⁻¹. The progressive loss of dissolved CO₂ concentration after a sample of water was poured into a goblet, may therefore be accessed by retrieving the following relationship:

$$c_L(t) = c_i - \frac{m(t)}{V} \quad (2)$$

with c_i being the initial concentration of dissolved CO₂ in water (given in Table 1), m(t) being the cumulative mass loss of CO₂ with time expressed in g, and V being the volume of water poured into the goblet expressed in L (namely 0.1 L in the present case).

Moreover, from a cumulative mass loss-time curve, the mass flux of CO₂ desorbing from the water surface (denoted F_{CO₂}) is

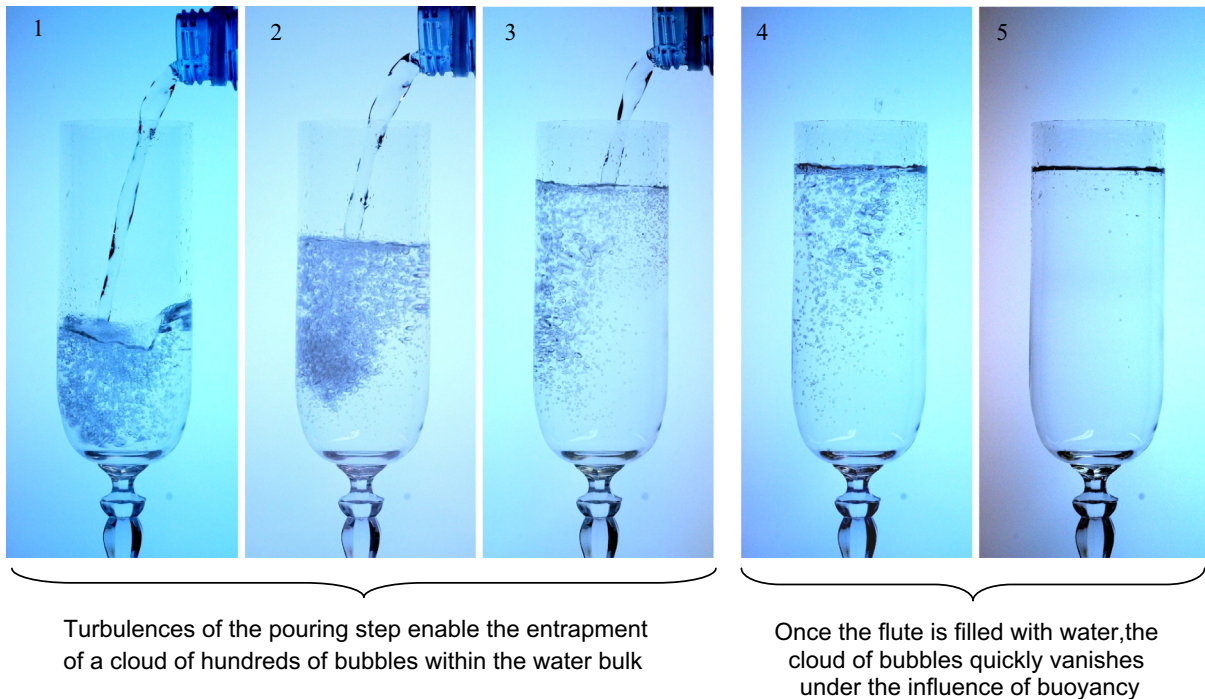


Fig. 1. During the pouring process, a cloud of bubbles forms, and progressively disappears as bubbles reach the free surface under the action of buoyancy.

therefore experimentally deduced all along the degassing process in the flute, by dividing the mass loss Δm by the time interval Δt between two data recordings (i.e., $F_{\text{CO}_2} = \Delta m / \Delta t$). During the tasting of a sparkling water (and a sparkling beverage in general), it is nevertheless indeed more pertinent to deal with volume fluxes rather than with mass fluxes of CO_2 . By considering the gaseous CO_2 desorbing out of water as an ideal gas, the experimental total volume flux of CO_2 (in $\text{cm}^3 \text{s}^{-1}$), denoted F_T , is therefore deduced as follows, all along the degassing process:

$$F_T = 10^6 \left(\frac{RT}{MP} \right) \frac{\Delta m}{\Delta t} \quad (3)$$

with R being the ideal gas constant (equal to $8.31 \text{ J K}^{-1} \text{ mol}^{-1}$), T being the water temperature (expressed in K), M being the molar mass of CO_2 (equal to 44 g mol^{-1}), P being the ambient pressure (close to 10^5 N m^{-2}), the loss of mass between two successive data records Δm being expressed in g, and Δt being the time interval between two data recordings (i.e., 5 s in the present case).

To enable a statistical treatment, four successive pouring and time series data recordings were done, for each type of water sample. At each step of the time series (i.e., every 5 s), an arithmetic average of the four data provided by the four successive time series corresponding to a single water sample was done, to finally produce one single “average” time series which is characteristic of a given water sample (but with standard deviations corresponding to the root-mean-square deviations of the values provided by the four successive data recordings).

2.5. Measuring the kinetics of bubbles growing stuck on a plastic goblet

$100 \pm 2 \text{ mL}$ of sparkling water were poured into a plastic goblet previously level-marked with 100 mL of distilled water. Immediately after pouring, the goblet was placed on a “cold” back-light table (identical to the one used to visualize the cloud of bubbles following the pouring process). Experiments were performed at room temperature ($20 \pm 1 \text{ }^\circ\text{C}$). Five minutes after pouring, bubbles growing stuck on the bottom of the plastic goblet were

monitored with time, through high-speed photography. A standard digital photo camera (NIKON D90) fitted with a MACRO objective (NIKKOR 60 mm) was used for this series of observation. The growth of bubbles’ diameters were monitored with time (during 30 s, i.e., from 5 min up to 5 min and 30 s after pouring the water into the goblet). It is worth noting that it was preferable to wait up to 5 min after pouring, since the liquid bulk is highly agitated during the first minutes following pouring (mainly due to the turbulences of the pouring step and the high bubbling activity) thus

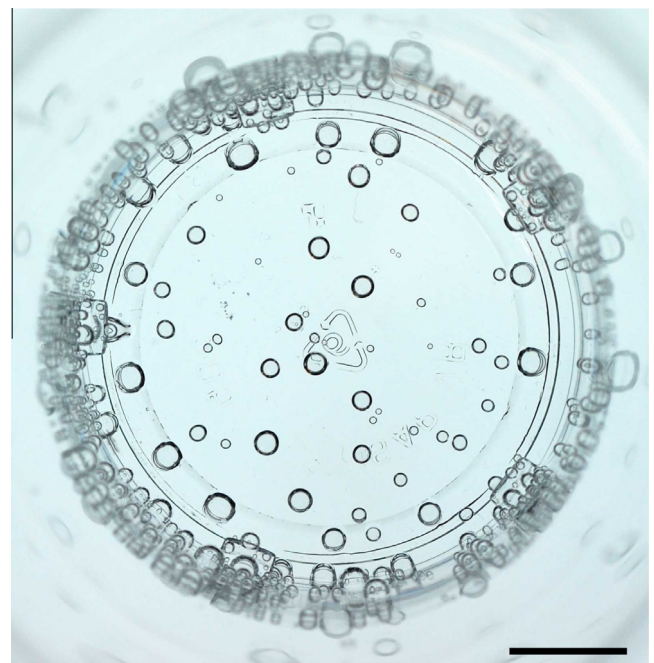


Fig. 2. A very typical photograph of bubbles growing stuck on the bottom of the plastic goblet (scale bar = 1 cm).

forbidding to focus accurately on bubbles stuck on the bottom of the goblet. It is also worth noting that a close inspection of successive frames must be done, in order to monitor exclusively the growth of bubbles growing by diffusion of CO₂ (and not by coalescence with neighboring bubbles, which would artificially increase the kinetics of bubble growth). A typical photograph of bubbles growing stuck on the bottom of the goblet is displayed in Fig. 2.

3. Results and discussion

3.1. The lifetime of quickly vanishing clouds of bubbles following pouring

Table 2 compiles the three so-called cloud of bubbles' lifetimes, for the three various water samples (together with their initial content of dissolved CO₂). The cloud of bubbles' lifetime accompanying pouring significantly varies from one water sample to another. The less dissolved CO₂ within the water, the longer the lifetime of the cloud. The cloud of bubbles has its origin as the sparkling water tongue impacts the bottom of the glass. Turbulences clearly trap tiny air bubbles into the water bulk. Moreover, flow patterns and eddies accompanying pouring certainly force the detachment of bubbles heterogeneously nucleated on the glass wall (Liger-Belair et al., 2010). All those bubbles get in the water bulk to feed the cloud. They will then grow in size by progressively accumulating dissolved CO₂ along their rise through buoyancy, to finally reach the water surface.

The ascending velocity U of a small, and single bubble, rising far from any boundary, obeys the following relationship:

$$U_{\text{Stokes}} = \frac{2\rho g}{9\eta} r^2 \quad (4)$$

where g is the gravity acceleration ($\approx 9.8 \text{ m s}^{-2}$), ρ is the density of water ($\approx 10^3 \text{ kg m}^{-3}$), and η is its dynamic viscosity (in Pa s).

Actually, a small bubble rising through a liquid phase supersaturated with dissolved CO₂ grows by diffusion, with a theoretical growth rate k expressed by the following relationship (see the recent review by Liger-Belair (2012), and references therein):

$$k = \frac{dr}{dt} \approx 0.63 \frac{RT}{P} D^{2/3} \left(\frac{2\rho g}{9\eta} \right)^{1/3} (c_L - c_0) \quad (5)$$

with R being the ideal gas constant ($8.31 \text{ J K}^{-1} \text{ mol}^{-1}$), T being the water temperature (expressed in K), P being the partial pressure of CO₂ within the bubble (close to 10^5 N m^{-2}), D being the diffusion coefficient of CO₂ molecules in sparkling water ($\approx 1.85 \times 10^{-9} \text{ m}^2 \text{ s}^{-1}$, as determined through ¹³C nuclear magnetic resonance (Liger-Belair et al., 2003)), c_L being the bulk concentration of dissolved CO₂ in the liquid phase (in mol m^{-3}), and c_0 being the concentration of dissolved CO₂ close to the bubble's interface, i.e., in Henry's equilibrium with gas phase CO₂ in the bubble ($c_0 = k_H P \approx 1.6 \text{ g L}^{-1} \approx 36 \text{ mol m}^{-3}$).

It is worth noting that the higher the bulk concentration of dissolved CO₂ in Eq. (5), the higher the growth rate of ascending bubbles (and therefore the larger the size of bubbles in the cloud of bubbles following pouring). The theoretical lifetime of the cloud of bubbles may therefore be approached by evaluating the time

needed for the smallest bubbles (with a negligible initial size) to travel the whole glass' height. It was stipulated indeed that the cloud of bubbles originates at the bottom of the glass. Bubbles therefore need to travel a distance, denoted h , equivalent to the level of water poured into the glass. By combining Eqs. (4) and (5), the following relationship is derived,

$$U = \frac{dh}{dt} \approx \frac{2\rho g}{9\eta} r^2 \approx \frac{2\rho g}{9\eta} (kt)^2 \quad (6)$$

which can be integrated as follows to access the characteristic time (denoted τ) needed for a bubble to travel a level of water denoted h before reaching the water surface:

$$\frac{2\rho g}{9\eta} k^2 \int_0^\tau t^2 dt \approx \int_0^h dh \quad (7)$$

By replacing in the latter equation k by its theoretical relationship given in Eq. (5), and by developing, the characteristic lifetime of the cloud of bubbles τ may be evaluated as:

$$\tau \approx 3 \left(\frac{\eta h}{2\rho g k^2} \right)^{1/3} \approx 4.5 \left(\frac{P}{RT} \right)^{2/3} \left(\frac{\eta}{\rho g} \right)^{5/9} \frac{h^{1/3}}{D^{4/9} (c_L - c_0)^{2/3}} \quad (8)$$

Under identical experimental conditions, the only parameter which differs from one water sample to another in Eq. (8) is the dissolved CO₂ concentration c_L . In Fig. 3, by replacing each parameter found in the latter equation by its numerical value, the theoretical lifetime τ was derived and is plotted vs. c_L , in the whole range of dissolved CO₂ concentrations covered in this study. Moreover, the experimentally determined cloud of bubbles' lifetimes are plotted in Fig. 3 as a function of the three respective dissolved CO₂ concentrations corresponding to each of the three various water samples. The general trend given by the theoretical model is in quite good agreement with our experimental results.

Nevertheless, it is worth noting that, due to cooperative effects, the velocity of small bubbles ascending close to each other in a cluster of bubbles may differ from the Stokes velocity expressed in Eq. (4). Therefore, the theoretical cloud of bubbles' lifetime based on the single bubble dynamics, and displayed in Eq. (8), should rather be seen as a first approach. By the way, the model

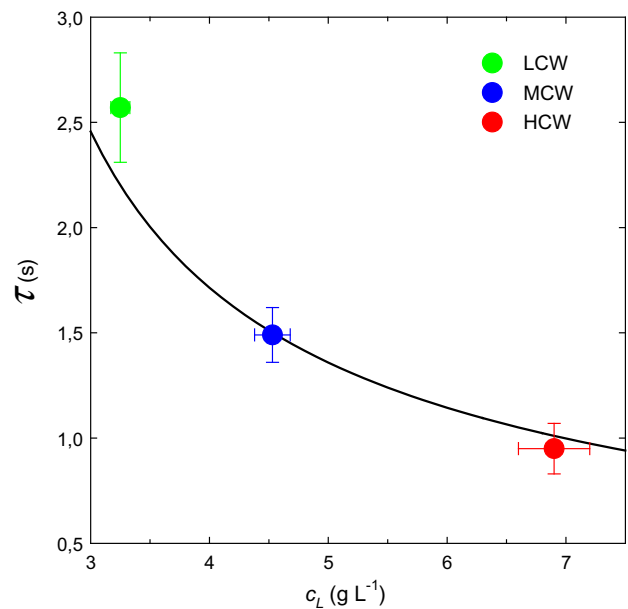


Fig. 3. Lifetime of the cloud of bubbles following pouring plotted as a function of the initial dissolved CO₂ concentration held in each of the three various carbonated water samples; the solid line is the theoretical lifetime modeled in Eq. (8).

Table 2
Lifetime of the cloud of bubbles following pouring, in relation with the initial dissolved CO₂ content found in each water sample.

Water sample	[CO ₂] c_L (g L^{-1})	Lifetime of the cloud of bubbles, t (s)
LCW	3.25 ± 0.08	2.57 ± 0.26
MCW	4.53 ± 0.15	1.49 ± 0.13
HCW	6.87 ± 0.28	0.95 ± 0.12

seems to deviate from experimental data with the LCW water sample. Moreover, due to different levels of dissolved CO₂, our three water samples show different clusters of bubbles during the pouring step (regarding the average bubble growth, the number of constituting bubbles, and finally the inter-bubble spacing). Taking into account all these parameters would add complexity in order to better describe the pouring step, which could indeed be the purpose of a future work, with a more stringent approach based on computer modeling.

3.2. The kinetics of dissolved CO₂ escaping from the water bulk after pouring

As long as the sparkling water bottle is hermetically closed, the capacity of a large quantity of gaseous CO₂ to remain dissolved in the liquid phase is achieved by the relatively high pressure of gas phase CO₂ in the bottle's headspace (through Henry's equilibrium). The situation is thermodynamically stable. But, as soon as the bottle is opened, and water is served into a glass, the thermodynamic equilibrium of gaseous CO₂ is broken. Dissolved CO₂ progressively escapes from the liquid phase to get in equilibrium with the partial pressure *P* of gaseous CO₂ in ambient air (of order of 0.4 mbar only). The corresponding new stable concentration of dissolved CO₂ is $c_{eq} = k_H P \approx 0.6 \text{ mg L}^{-1}$ only (following Henry's law, at 20 °C). Suffice to say that almost all dissolved CO₂ initially held by sparkling water must desorb from the liquid phase. This progressive desorption is usually achieved after several hours. It is worth noting that dissolved CO₂ escapes from the sparkling water into the form of heterogeneously nucleated bubbles, but also by "invisible" diffusion, through the free air/water interface (see Fig. 4). In Fig. 5, the progressive decrease of dissolved CO₂ concentrations in the three various water samples are displayed with

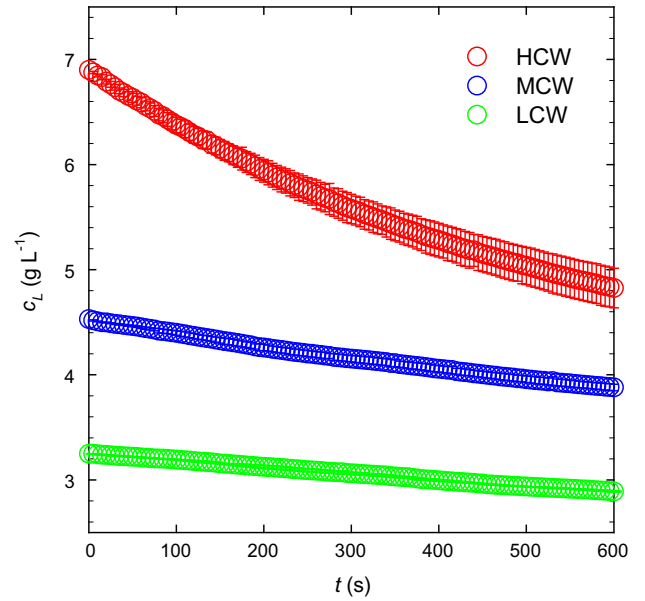


Fig. 5. Progressive losses of dissolved CO₂ concentrations (in g L⁻¹) with time, as determined with Eq. (2), from 100 mL of each of the three carbonated water samples poured in the plastic goblet.

time, all along the first 10 min following the pouring process. Quite logically, it is clear from Fig. 5 that the higher the initial dissolved CO₂ level is, the more rapid the corresponding loss of dissolved CO₂ is. Nevertheless, it is worth noting that the concentration of dissolved CO₂ constantly remains higher in the HCW water, which holds the highest initial concentration of dissolved CO₂, all along the first 10 min following pouring. This set of analytical data correlating the progressive loss of dissolved CO₂ from a carbonated water with time (under standard tasting conditions) could be of interest for consumers. Depending on the intensity of the tingling sensation promoted by dissolved CO₂ in mouth, the time to wait after pouring could be deduced, for a given water type (depending on its initial level of dissolved CO₂).

Invisible diffusion of dissolved CO₂ through the water surface

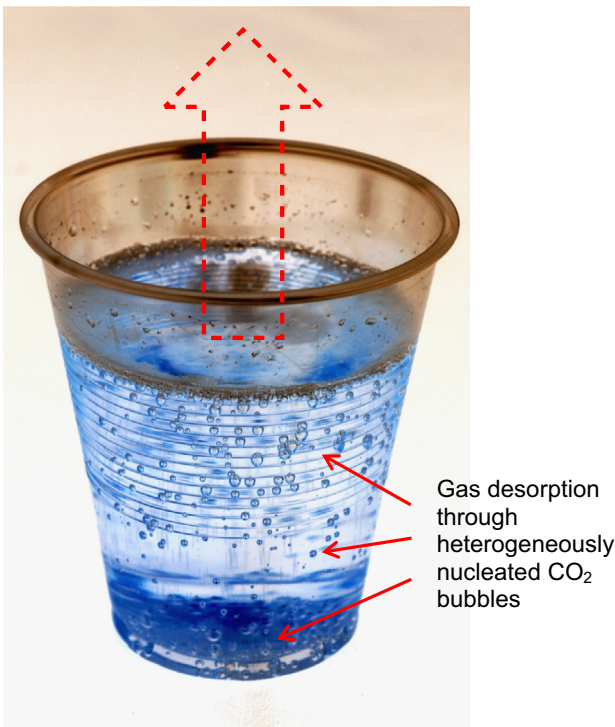


Fig. 4. When poured in a goblet, dissolved CO₂ escapes the liquid phase through (i) heterogeneously nucleated bubbles, and through (ii) the water free surface.

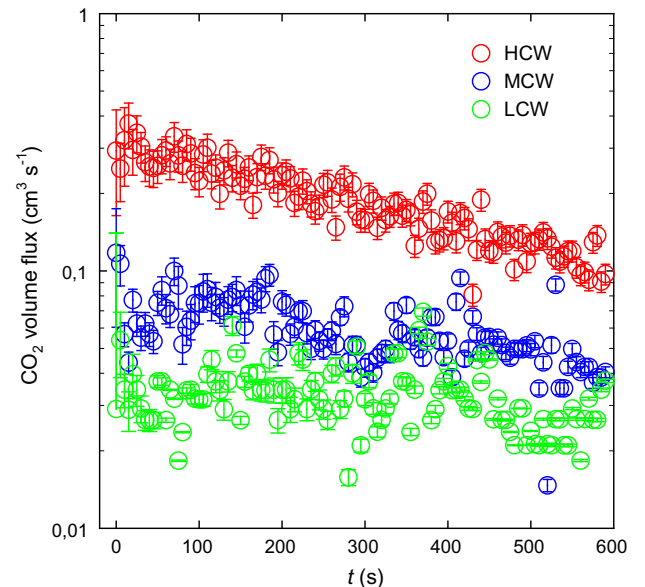


Fig. 6. Gaseous CO₂ volume fluxes (in cm³ s⁻¹) desorbing with time, as determined with Eq. (3), from 100 mL of a carbonated water sample poured in the plastic goblet.

Moreover, another pertinent analytical parameter which characterizes the release of CO₂ from a sparkling beverage is the volume flux of gaseous CO₂ escaping from the air/liquid interface (Mulier et al., 2009; Liger-Belair et al., 2013). Fig. 6 shows average CO₂ volume fluxes outgassing from the goblet poured with the three samples of various waters, respectively, as determined with Eq. (3). Moreover, since the driving force behind the desorption of dissolved gas species from a supersaturated liquid phase is its bulk concentration of dissolved CO₂ (Liger-Belair et al., 2013), it seemed pertinent to propose a correlation between the CO₂ volume flux outgassing from a goblet poured with sparkling water and the continuously decreasing bulk concentration of dissolved CO₂. To do so, time series data recordings displayed in Figs. 5 and 6 were combined. Time was eliminated so that the CO₂ volume flux outgassing from the goblet was plotted as a function of c_L . Correlations between total CO₂ volume fluxes outgassing from the goblet and dissolved CO₂ concentrations found in the carbonated water are displayed in Fig. 7. It is evident from Fig. 7, that the three various sparkling water samples explore three significantly different zones of dissolved CO₂ concentrations, and therefore clearly differentiate from one another from an analytical point of view.

3.3. The kinetics of bubbles growing stuck on a plastic goblet

3.3.1. Required background

Bubbles stuck on the bottom of the plastic goblet are considered as portions of spherical caps, with a radius r and a volume $v \propto r^3$. Gaseous CO₂ inside a bubble is considered as an ideal gas, which therefore obeys the following relationship:

$$Pv = nRT \quad (9)$$

with P being the pressure, and n the number of gaseous CO₂ moles inside the bubble.

Due to the spherical geometry of the bubble, the variation of the number of moles which crosses the bubble interface per unit of time therefore obeys the following relationship:

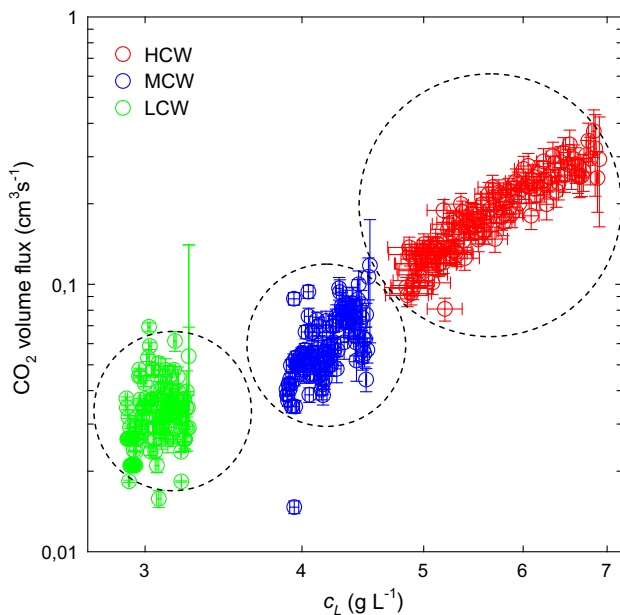


Fig. 7. Gaseous CO₂ volume fluxes (in cm³ s⁻¹) desorbing with time as a function of the dissolved CO₂ concentration (in g L⁻¹) found in 100 mL of a carbonated water sample poured in the plastic goblet; standard deviations correspond to the root-mean-square deviations of the values provided by the four successive data recordings.

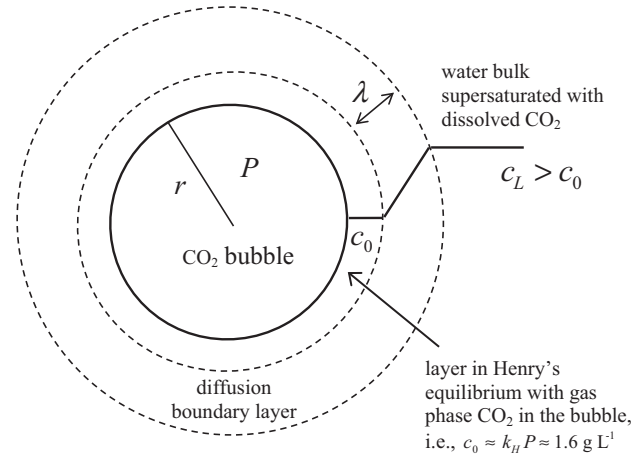


Fig. 8. Close to the bubble interface, the concentration of dissolved CO₂ is in equilibrium with gas phase CO₂ into the bubble and equals c_0 ; far from the bubble interface, the concentration of dissolved CO₂ equals that of the liquid bulk c_L ; in the diffusion boundary layer between, a gradient of dissolved CO₂ exists, which is the driving mechanism behind diffusion of dissolved CO₂ and bubble growth.

$$\frac{dn}{dt} \approx \frac{P}{RT} \frac{dv}{dt} \propto \frac{P}{RT} r^2 \frac{dr}{dt} \quad (10)$$

The mechanism behind the growth of a bubble being molecular diffusion, the flux J of gaseous CO₂ which crosses the bubble interface obeys the so-called Fick's law, which stipulates that:

$$J = -D\nabla c \approx D \frac{\Delta c}{\lambda} \quad (11)$$

with D being the diffusion coefficient of CO₂ molecules in water, $\Delta c = c_L - c_0$ being the dissolved CO₂ molar concentration difference between the water bulk and the bubble interface in Henry's equilibrium with gas phase CO₂ in the bubble (see Fig. 8), and λ being the thickness of the diffuse boundary layer where the gradient of dissolved CO₂ concentration exists. Therefore, due to the spherical geometry of the bubble, the number of CO₂ moles which crosses the bubble interface per unit of time is:

$$\frac{dn}{dt} \propto r^2 J \propto r^2 D \frac{\Delta c}{\lambda} \quad (12)$$

Generally speaking, diffusion of dissolved gas species may be ruled by (i) pure diffusion or by (ii) diffusion-convection, whether the liquid phase is perfectly stagnant or in motion (Incropera et al., 2007). The two aforementioned situations must therefore, *a priori*, be taken into account in our discussion.

3.3.1.1. Pure diffusion. In a purely diffusive case, a boundary layer depleted with dissolved gas molecules progressively expands near the bubble interface, i.e., λ progressively increases, so that the diffusion of gas species desorbing from the liquid bulk inexorably and quickly slows down. In case of a spherical geometry, the boundary layer depleted with dissolved CO₂ progressively expands around the bubble cap, in the form of a portion of spherical shell with a thickness λ . The mass conservation between the diffuse boundary layer and the spherical bubble cap may therefore be written as:

$$dn \propto (r + \lambda)^2 d\lambda \Delta c \quad (13)$$

By combining Eqs. (12) and (13) and by integrating, the progressive growth of the diffuse boundary layer may be deduced as time proceeds as follows:

$$\begin{cases} \lambda_{ST} \approx (Dt)^{1/2} & \text{for short times, i.e., } \lambda \ll r \\ \lambda_{LG} \approx r^{1/2} (Dt)^{1/4} & \text{for long times, i.e., } \lambda \gg r \end{cases} \quad (14)$$

Finally, by combining Eqs. (10), (12) and (14) and by integrating, the progressive growth of the spherical bubble cap growing by pure diffusion may be deduced through the following relationships:

$$\begin{cases} r(t) \approx \frac{RT\Delta c}{P} (Dt)^{1/2} & \text{for short times, i.e., } \lambda \ll r \\ r(t) \approx \left(\frac{RT\Delta c}{P}\right)^{2/3} (Dt)^{1/2} & \text{for long times, i.e., } \lambda \gg r \end{cases} \quad (15)$$

Finally, in case of a bubble growing stuck on the glass wall by pure diffusion, the bubble radius increases proportionally to the square root of time, i.e., $\propto t^{1/2}$, as demonstrated in the pioneering work done by Scriven, and conducted with a spherically capped bubble growing by pure diffusion on a solid substrate (Scriven, 1959).

3.3.1.2. When convection plays its part. In case of a liquid medium agitated with flow patterns, convection forbids the growing of the diffusion boundary layer, thus keeping it roughly constant by continuously supplying the liquid around the bubble with dissolved CO₂ freshly renewed from the liquid bulk.

By combining Eqs. (10) and (12) (with λ being constant), and by integrating, the progressive growth of the spherical bubble cap growing under natural convection conditions may be deduced through the following relationships:

$$r(t) \propto \frac{RTD}{P} \frac{\Delta c}{\lambda} t \quad (16)$$

Finally, in case of a bubble growing under convection conditions, the bubble radius increases linearly with time, i.e., $\propto t$. Therefore, by closely examining the kinetics of a bubble growth (via the critical exponent of the dependence of bubbles' radii with time), it is therefore possible to determine whether bubbles grow by pure diffusion or under convection conditions.

3.3.2. Experimental results and discussion

A series of snapshots showing the progressive growth of bubbles stuck on the bottom of a plastic goblet poured with HCW (during a 30 s period of time) are displayed in Fig. 9. A close examination of the time sequence displayed in Fig. 9 shows several coalescence events between bubbles growing close to each other. Coalescence events artificially increase the growth rate of bubbles, and therefore the average bubble size distribution on the bottom of the goblet. Moreover, it is also worth noting that bubbles growing very close to each other, but without coalescing, show growth rates much smaller than single bubbles growing far from their neighbors (see Fig. 10). In such cases, bubbles compete with each other for dissolved CO₂. Actually, bubbles literally “feed” with dissolved CO₂ coming from the same environment, which contributes to decrease their respective growth rates. No doubt from the close exam of growing bubbles displayed in Fig. 10 that, in the same period of time, the single bubble (S) grows faster than the three bubbles growing close to each other. This observation is indeed self-consistent with a recent one done by Enriquez et al. (2013) in an aqueous solution slightly supersaturated with carbon dioxide. In this work, authors reported that the growth rate of a pair of bubbles growing close to each other is slightly slower than the single bubble case, thus suggesting that each bubble in the pair influences the growth rate of the other bubble (Enriquez et al., 2013).

In order to compare the respective bubble growth rates with each other in the various water samples, the progressive increase of various bubble diameters was systematically followed with time (for single bubbles growing as far as possible from neighboring bubbles, to prevent both coalescence and competition with regard to diffusion of dissolved CO₂). Fig. 11 compiles three various

kinetics of bubble diameters increase with time (during a 30 s period of time, and 5 min after pouring) in the three various carbonated water samples. The general trend of data series unambiguously shows that bubble diameters increase linearly with time, thus confirming the likely growth of CO₂ bubbles under convection conditions, as expressed in Eq. (16). It is indeed not really surprising to realize that bubbles stuck on the bottom of the plastic goblet grow under convection conditions. Actually, bubbles continuously detach from the plastic wall (through buoyancy), thus disturbing the whole water bulk with continuously renewed convection patterns, which forbid the growing of the diffuse boundary layer and keeping it roughly constant around the bubble.

Such a growing under convection conditions has already been observed for heterogeneously nucleated bubbles in a glass of champagne (Liger-Belair et al., 2006). Nevertheless, and most interestingly, it is worth noting that, in the work by Barker et al. (2002), the growth rate of CO₂ bubbles following depressurisation of a saturated CO₂/water solution was not constant with time, despite dissolved CO₂ concentrations comparable as those found in our set of experiments (i.e., several grams per liter). In the time data series compiled by Barker et al. (2002), bubble diameters rather followed a trend proportional to the square root of time, as in the purely diffusive case presented in the above section. Why such a difference of scaling law, despite comparable dissolved CO₂ concentrations in both studies?

We are tempted to propose an explanation based on the liquid phase around CO₂ bubbles growing by diffusion. Actually, in the work by Barker et al. (2002), before the sudden depressurisation of the CO₂/water solution, the liquid phase is indeed perfectly stagnant, and therefore at rest. Bubbles therefore nucleate and grow in a liquid environment free from convection, thus leading to pure diffusion conditions (i.e., with a diffusion boundary layer growing around bubbles as the zone around bubbles progressively gets depleted with dissolved CO₂). In our situation, under standard tasting conditions, the bubbling environment (i.e., bubbles detaching periodically from the plastic goblet) continuously drives flow patterns around bubbles growing stuck on the plastic goblet. The liquid phase is far from being stagnant, thus keeping the diffusion boundary layer roughly constant, and therefore forbidding purely diffusive conditions for bubble growth.

In our set of diameters vs. time data series, bubble growth rates may easily be accessed by linearly fitting bubbles diameter increase with time (see Fig. 11 which compiles three various diameters vs. time data series, in the three water samples). The slope of each data series therefore corresponds to the experimental growth rate, denoted $k = dr/dt$, of a given bubble growing in the corresponding water sample. As seen in Fig. 11, the three various water samples experience significantly different bubble growth rates. Logically, and as could have been expected, the higher the concentration of dissolved CO₂ in the water bulk is, the more rapidly a bubble expands. Moreover, and following the theoretical relationship (16), the slopes of the various diameters vs. time data series correspond to the theoretical prefactor in Eq. (16), i.e., $\frac{RTD\Delta c}{P\lambda}$. The only unknown parameter in this prefactor is the thickness λ of the diffuse boundary layer (kept roughly constant under convection conditions). Interestingly, the thickness of the diffuse boundary layer may therefore indirectly be approached in each water sample by equaling this theoretical prefactor with corresponding experimental bubble growth rates k as follows:

$$\lambda \approx \frac{RTD}{P} \frac{\Delta c}{k} \quad (17)$$

By replacing in Eq. (17) each parameter by its numerical value, the thickness of the diffuse boundary layer has been determined for each carbonated water sample. It is worth noting that, because experimental growth rates k have been determined for bubbles

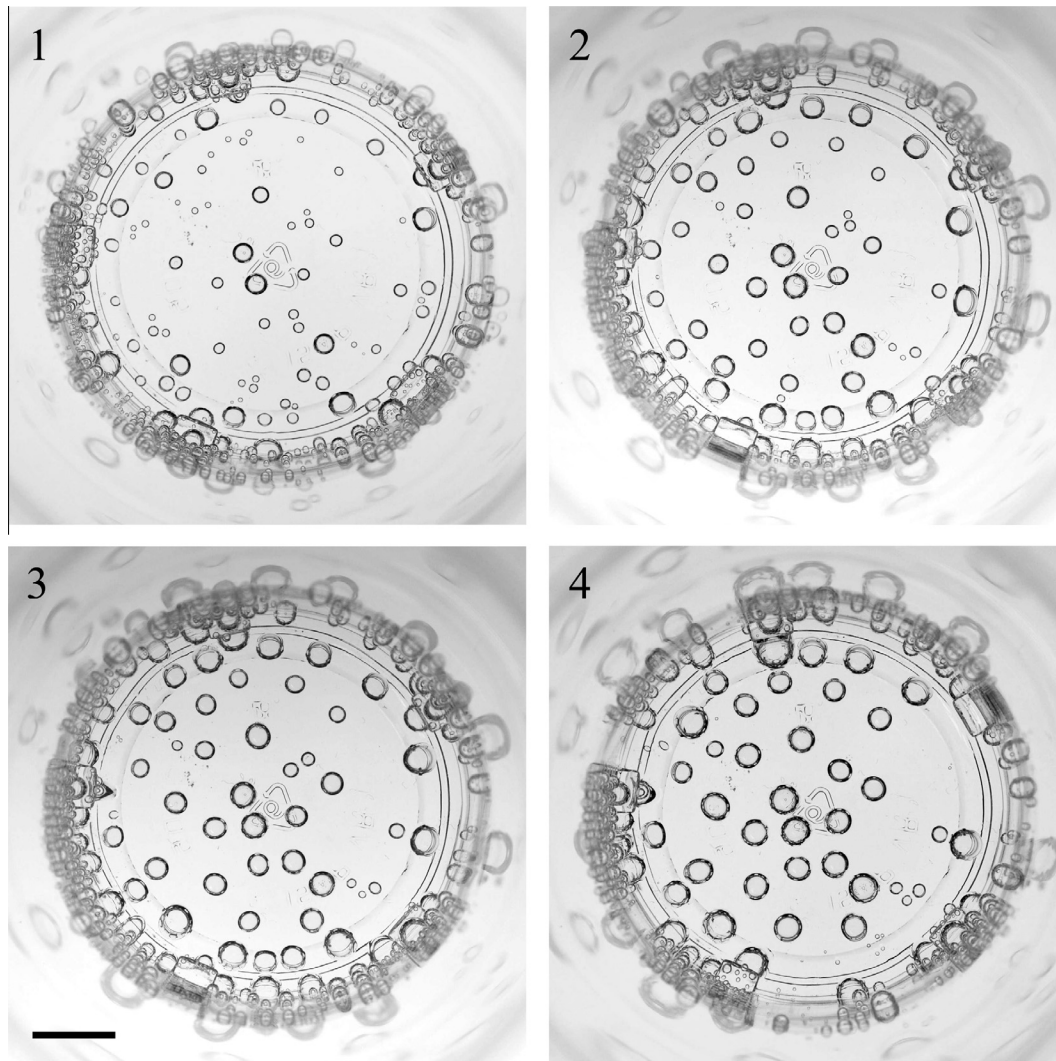


Fig. 9. Time sequence showing bubbles growing stuck on the bottom of the plastic goblet poured with the HCW carbonated water sample; the time interval between successive frames is 10 s (scale bar = 1 cm).

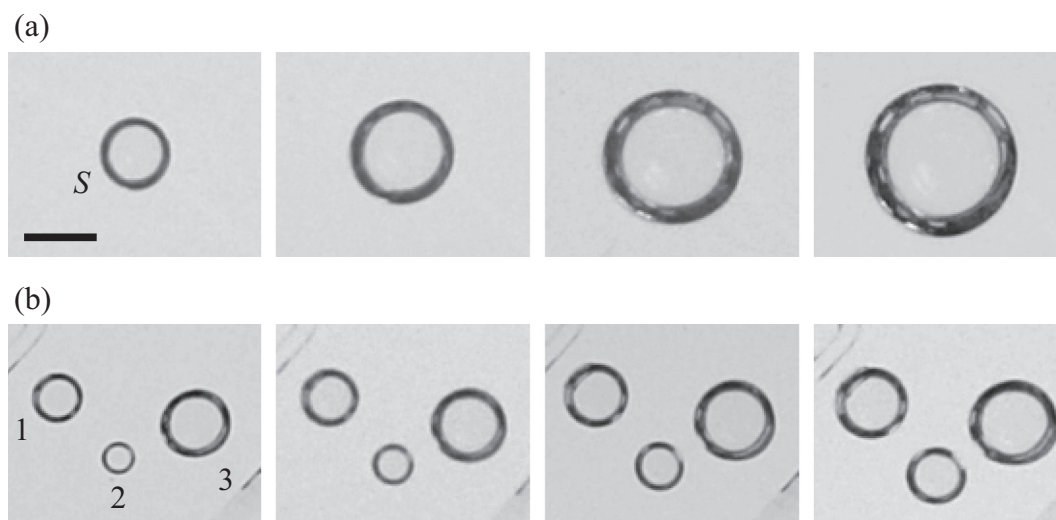


Fig. 10. Time sequences extracted from the same global time sequence displayed in Fig. 9, aiming to compare the growth rates of different bubbles stuck on the bottom of the plastic goblet; no doubt that the diameter of the single bubble far from neighboring bubbles (a), grows faster than the diameters of the three bubbles growing close to each other's (b); the time interval between successive frames is 10 s (scale bar = 1 mm).

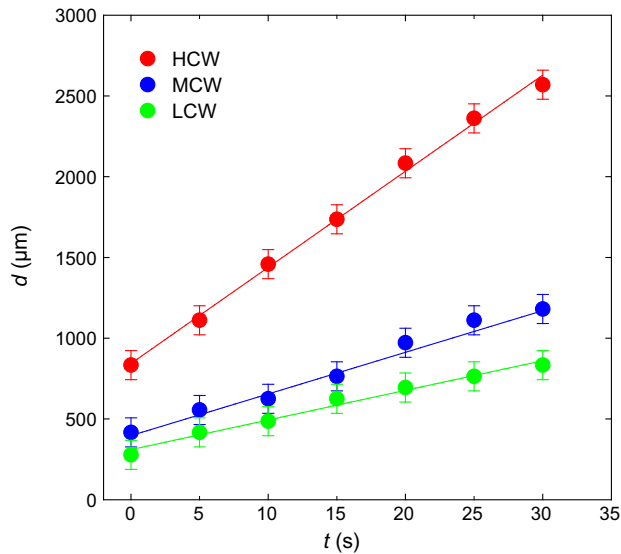


Fig. 11. Bubble diameter vs. time, for single bubbles (far from neighboring bubbles) growing stuck on the bottom of the plastic goblet, 5 min after pouring; the growth rate of bubbles from the three various carbonated water samples were compared with each other's.

Table 3

Experimental bubble growth rates, and corresponding thickness of the diffusion boundary layer around the growing bubble (following Eq. (16)), 5 min after pouring, in relation with the difference in dissolved CO₂ between the water bulk and the bubble surface in Henry's equilibrium with gas phase CO₂ within the bubble.

Water sample	$\Delta c = c_L - c_0$ (5 min after pouring, g L ⁻¹)	Bubble growth rate, k (μm s ⁻¹)	Diffusion boundary layer thickness, λ (μm)
LCW	1.46 ± 0.09	9 ± 2	166 ± 47
MCW	2.55 ± 0.18	13 ± 2	201 ± 45
HCW	3.98 ± 0.42	28 ± 6	146 ± 47

growing stuck on the plastic goblet 5 min after pouring, Δc in Eq. (17) should also be determined 5 min after pouring water in the goblet (through the losses of dissolved CO₂ with time given in Fig. 5 for the three carbonated water samples). Table 3 compiles the pertinent data needed to reasonably approach λ in the three carbonated water samples. The thicknesses of diffuse boundary layers were found to be of order of 100–200 μm around bubbles growing stuck on the plastic goblet.

4. Conclusions and prospects

The three commercial bottled carbonated natural mineral waters investigated in this study clearly showed very significant differences regarding their bubbling behavior, as well as their kinetics of dissolved CO₂ escaping the water bulk, under standard tasting conditions. It was clearly demonstrated that, the higher the concentration of dissolved CO₂ initially found in the water bulk, (1) the lower the lifetime of the cloud of bubbles following pouring, (2) the higher the kinetics of dissolved CO₂ discharging from the water bulk (as well as corresponding volume fluxes of gaseous CO₂ outgassing from the goblet), and (3) the more rapidly bubbles expand when stuck on the plastic goblet. No wonder that all those differences, evidenced under standard tasting conditions, should impact the sensory properties experienced by a consumer enjoying a glass of carbonated water. Moreover, by combining classical ascending bubble dynamics with mass transfer considerations, a multi-parameter modeling was proposed, which links the lifetime of clouds of bubbles following pouring with several parameters of the liquid phase and the glass itself. Moreover and interestingly, 5 min after pouring, the diameter of bubbles stuck

on a plastic goblet was found to increase linearly with time (i.e., with $d \propto t$), thus betraying a diffusion process of dissolved CO₂ from the water bulk to the bubbles operating under convection conditions (likely because bubbles continuously detaching from the plastic goblet give rise to renewed flow patterns in the water bulk, thus forbidding the growing of the diffuse boundary layer around the bubbles).

These experimental observations and theoretical developments, relevant to common situations involving the service of commercial sparkling bottled waters, could certainly be extended more generally to the very large area of non-alcoholic sparkling beverages, also looking for new insights and novelties. Bubbles dynamics in sparkling alcoholic beverages have indeed been widely investigated in the past decade, mainly with champagne, sparkling wines, and beers, whereas several commercial sparkling bottled waters were hereby analyzed. Non-alcoholic sparkling beverages such as soft drinks, which can be viewed (regarding their chemical complexity) as intermediate between sparkling alcoholic beverages and sparkling waters, could also certainly benefit from further development regarding bubble dynamics and gas-solution thermodynamics.

Acknowledgments

G rard Liger-Belair and Clara Cilindre are indebted to the Europ l'Agro institute, the Association Recherche Oenologie Champagne Universit , the CNRS, the R gion Champagne-Ardenne, the Ville de Reims, and the Conseil G n ral de la Marne for supporting their team and research.

References

- Barker, G.S., Jefferson, B., Judd, S.J., 2002. The control of bubbles in carbonated beverages. *Chem. Eng. Sci.* 57, 565–573.
- Bruce, B., 2013. Growth potential for global bottled water industry. <<http://www.foodbev.com/news/growth-potential-for-global-bottled-water#VCq-d74WmJY>>.
- Cain, W.S., Murphy, C.L., 1980. Interaction between chemoreceptive modalities of odour and irritation. *Nature* 284, 255–257.
- Calderone, G., Guillou, C., Reniero, F., Naulet, N., 2007. Helping to authenticate sparkling drinks with ¹³C/¹²C of CO₂ by gas chromatography–isotope ratio mass spectrometry. *Food Res. Int.* 40, 324–331.
- Caputi, A., Ueda, M., Walter, P., Brown, T., 1970. Titrimetric determination of carbon dioxide in wine. *Am. J. Enol. Viticult.* 21, 140–144.
- Carroll, J.J., Mather, A.E., 1992. The system carbon dioxide/water and the Krichevsky–Kasarnovsky equation. *J. Solution Chem.* 21, 607–621.
- Chandrashekar, J., Yarmolinsky, D., von Buchholtz, L., Oka, Y., Sly, W., Ryba, N.J., Zucker, C.S., 2009. The taste of carbonation. *Science* 326, 443–445.
- Cometto-Muniz, J.E., Garcia-Medina, M.R., Calvino, A.M., Noriega, G., 1987. Interactions between CO₂ oral pungency and taste. *Perception* 16, 629–640.
- Dessirier, J.M., Simons, C., Carstens, M., O'Mahony, M., Carstens, E., 2000. Psychophysical and neurobiological evidence that the oral sensation elicited by carbonated water is of chemogenic origin. *Chem. Senses* 25, 277–284.
- Diamond, L.W., Akinfiev, N.N., 2003. Solubility of CO₂ in water from 1.5 to 100 °C and from 0.1 to 100 MPa: evaluation of literature data and thermodynamic modelling. *Fluid Phase Equilib.* 208, 265–290.
- Directive 2009/54/EC of the European parliament and of the council of 18 June 2009 on the exploitation and marketing of natural mineral waters.
- Dunkel, A., Hofmann, T., 2010. Carbonic anhydrase IV mediates the fizz of carbonated beverages. *Angewandte Chemie – Int. Ed.* 49, 2975–2977.
- Enriquez, O.R., Hummelink, C., Bruggert, G.-W., Lohse, D., Prosperetti, A., van der Meer, D., Sun, C., 2013. Growing bubbles in a slightly supersaturated liquid solution. *Rev. Sci. Instrum.* 84, 065111.
- Euzen, A., 2006. Bottled water, globalization and behaviour of consumers. *Eur. J. Water Qual.* 37, 143–155.
- Forbes, 2014. <<http://www.forbes.com/sites/greatspeculations/2014/01/14/coca-cola-eyes-growth-in-the-sparkling-bottled-water-market/>>.
- Gleick, P.H., 2010. *Bottled and Sold: The Story behind Our Obsession with Bottled Water*. Island Press, Washington.
- Incropera, F., Dewitt, D., Bergman, T., Lavine, A., 2007. *Fundamentals of Heat and Mass Transfers*. Wiley, New York.
- Jones, S.F., Evans, G.M., Galvin, K.P., 1999. Bubble nucleation from gas cavities: a review. *Adv. Colloid Interface Sci.* 80, 27–50.
- Kleeman, A., Albrecht, J., Schöpf, V., Haegler, K., Kopietz, R., Hempel, J.M., Linn, J., Flanagan, V.L., Fesl, G., Wiesmann, M., 2009. Trigeminal perception is necessary to localize odors. *Physiol. Behav.* 97, 401–405.

- Lawless, H.T., Heymann, H., 2010. *Sensory Evaluation of Food: Principles and Practices*. Springer, New York.
- Liger-Belair, G., Prost, E., Parmentier, M., Jeandet, P., Nuzillard, J.-M., 2003. Diffusion coefficient of CO₂ molecules as determined by ¹³C NMR in various carbonated beverages. *J. Agric. Food Chem.* 51, 7560–7563.
- Liger-Belair, G., Parmentier, M., Jeandet, P., 2006. Modeling the kinetics of bubble nucleation in champagne and carbonated beverages. *J. Phys. Chem. B* 110, 21145–21151.
- Liger-Belair, G., Villaume, S., Cilindre, C., Jeandet, P., 2009. Kinetics of CO₂ fluxes outgassing from champagne glasses in tasting conditions: the role of temperature. *J. Agric. Food Chem.* 57, 1997–2003.
- Liger-Belair, G., Bourget, M., Villaume, S., Jeandet, P., Pron, H., Polidori, G., 2010. On the losses of dissolved CO₂ during champagne serving. *J. Agric. Food Chem.* 58, 8768–8775.
- Liger-Belair, G., Conreux, A., Villaume, S., Cilindre, C., 2013. Monitoring the losses of dissolved carbon dioxide from laser-etched champagne glasses. *Food Res. Int.* 54, 516–522.
- Liger-Belair, G., 2012. The physics behind the fizz in Champagne and sparkling wines. *Eur. Phys. J. Spec. Top.* 201, 1–88.
- Liger-Belair, G., 2014. How many bubbles in your glass of bubbly? *J. Phys. Chem. B* 118, 3156–3163.
- Lubetkin, S.D., 2003. Why is it much easier to nucleate gas bubbles than theory predicts? *Langmuir* 19, 2575–2587.
- Meusel, T., Negoias, S., Scheibe, M., Hummel, T., 2010. Topographical differences in distribution and responsiveness of trigeminal sensitivity within the human nasal mucosa. *Pain* 151, 516–521.
- Mulier, M., Zeninari, V., Joly, L., Decarpenterie, T., Parvitte, B., Jeandet, P., Liger-Belair, G., 2009. Development of a compact CO₂ sensor based on near-infrared laser technology for enological applications. *Appl. Phys. B: Lasers Optics* 94, 725–733.
- Rani, B., Maheshwari, R., Garg, A., Prasad, M., 2012. Bottled water – a global market overview. *Bull. Environ. Pharmacol. Life Sci.* 1 (6), 1–4.
- Rodwan, J.G., 2012. Bottled water 2011: the recovery continues. *Bottled Water Recovery (BWR)* April/May, 12–21.
- Scriven, L.E., 1959. On the dynamics of phase growth. *Chem. Eng. Sci.* 10, 1–13.
- Storey, M., 2010. The shifting beverage landscape. *Physiol. Behav.* 100, 10–14.
- Wilt, P.M., 1986. Nucleation rates and bubble stability in water-carbon dioxide solutions. *J. Colloid Interface Sci.* 112, 530–538.
- Wise, P.M., Wolf, M., Thom, S.R., Bryant, B., 2013. The influence of bubbles on the perception carbonation bite. *PLoS ONE* 8, e71488.